cPKC regulates interphase nuclear size during *Xenopus* development

Lisa J. Edens and Daniel L. Levy

Department of Molecular Biology, University of Wyoming, Laramie, WY 82071

Dramatic changes in cell and nuclear size occur during development and differentiation, and aberrant nuclear size is associated with many disease states. However, the mechanisms that regulate nuclear size are largely unknown. A robust system for investigating nuclear size is early *Xenopus laevis* development, during which reductions in nuclear size occur without changes in DNA content. To identify cellular factors that regulate nuclear size during development, we developed a novel nuclear resizing assay wherein nuclei assembled in *Xenopus* egg extract become smaller in the presence of cytoplasmic interphase extract isolated from post-gastrula *Xenopus* embryos. We show that nuclear shrinkage depends on conventional protein kinase C (cPKC). Increased nuclear cPKC localization and activity and decreased nuclear association of lamins mediate nuclear size reductions during development, and manipulating cPKC activity in vivo during interphase alters nuclear size in the embryo. We propose a model of steady-state nuclear size regulation whereby nuclear expansion is balanced by an active cPKC-dependent mechanism that reduces nuclear size.

Introduction

It has long been known that the size of the nucleus varies dramatically among different species, cell types, and developmental stages (Webster et al., 2009; Edens et al., 2013). Aberrant nuclear size is associated with certain disease states, and the diagnosis and prognosis of many cancers is based on graded increases in nuclear size (Blom et al., 1990; Zink et al., 2004; Dey, 2010; Jevtić and Levy, 2014). While development, differentiation, and cancer are associated with changes in nuclear size, global chromatin organization, and gene expression, the interplay between these parameters is unclear (Meshorer and Misteli, 2006; Dekker et al., 2013). Addressing these issues necessitates an understanding of mechanisms of nuclear size regulation.

Although manipulating the levels or activities of nuclear envelope (NE) components can alter the size and shape of the nucleus (Sims et al., 1992; Webster et al., 2009; Levy and Heald, 2012; Edens et al., 2013; Jevtić et al., 2014), relatively few studies address mechanisms of nuclear size regulation in a physiological context. Early *Xenopus laevis* development is a robust system for investigating mechanisms of nuclear size regulation. Upon fertilization, the *X. laevis* single-cell embryo (∼1 mm diameter) undergoes a series of 12 rapid cell divisions (stages 1–8) to generate several thousand 50-µm-diameter and smaller cells, reaching a developmental stage termed the midblastula transition (MBT), or stage 8.5 (Nieuwkoop and Faber, 1956). The MBT is characterized by slower, asynchronous cell divisions and the onset of zygotic transcription (Newport and Kirschner, 1982a,b). In pre-MBT embryos, nuclei expand continuously throughout interphase. Around the MBT, durations of interphase increase, rates of nuclear expansion slow, and nuclei stop growing within interphase, reaching a steady-state size (Levy and Heald, 2010). In addition to this change in nuclear dynamics, post-MBT nuclear size scales smaller without changes in nuclear DNA content (Fig. 1 A).

Nothing is known mechanistically about what accounts for the threefold decrease in NE surface area from the MBT (stage 8.5) to gastrulation (stages 10.5–12) or why interphase nuclear growth stops to reach a steady-state size (Gerhart, 1980; Levy and Heald, 2010). Because *Xenopus* egg and embryo extracts have been extensively used to study the nucleus and mechanisms of organelle size regulation (Chan and Forbes, 2006; Edens and Levy, 2014), we adapted this system to elucidate mechanisms of nuclear size regulation in the post-MBT *Xenopus* embryo. We developed an in vitro assay wherein large

The Rockefeller University Press $30.00
J. Cell Biol. Vol. 206 No. 4   473–483
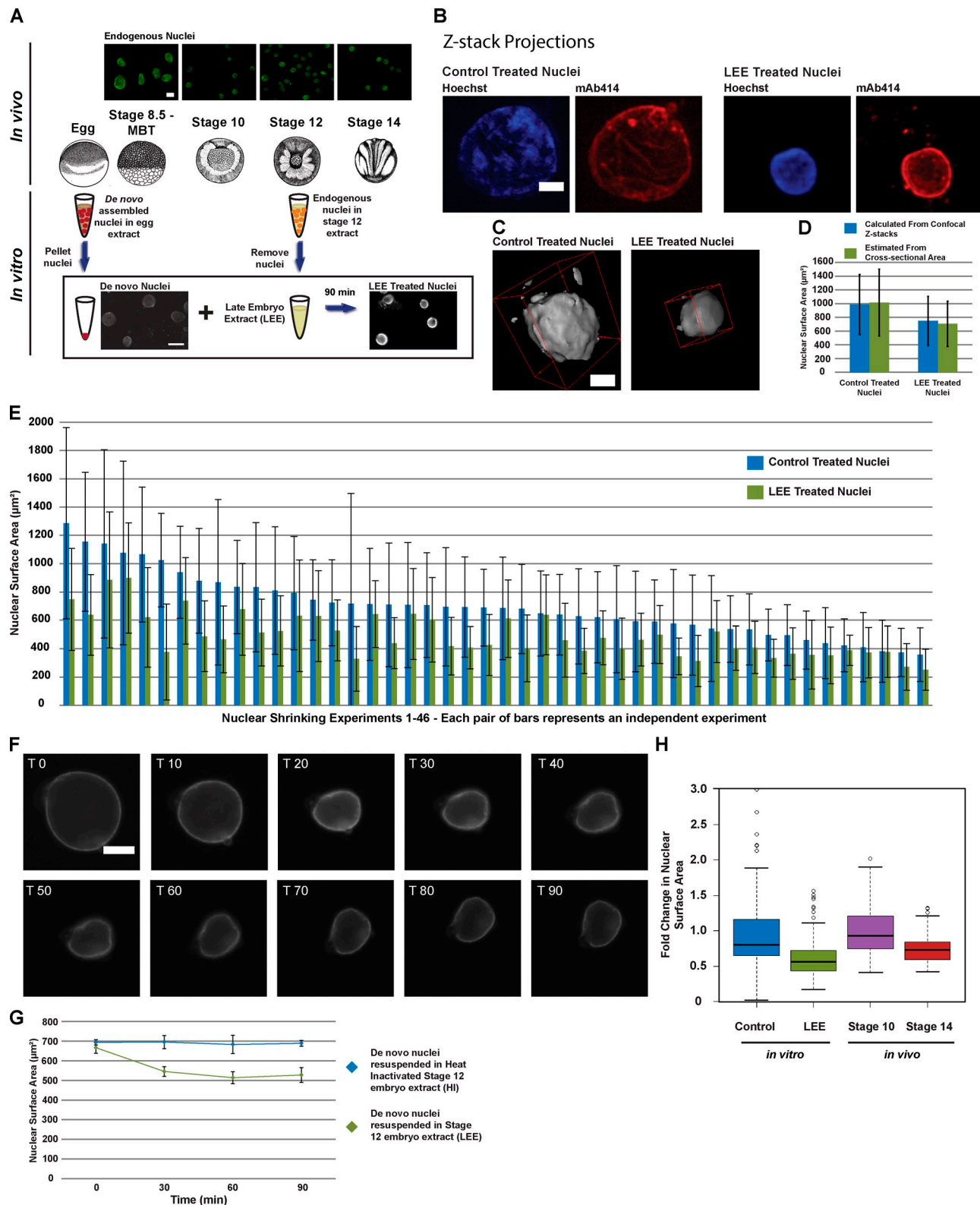www.jcb.org/cgi/doi/10.1083/jcb.201406004

JCB   473

Figure 1. **Characterization of a novel nuclear shrinking assay.** (A) In vivo: diagrams of *X. laevis* embryos are reprinted from Nieuwkoop and Faber (1956), and images of NPC-stained endogenous embryonic nuclei are adapted from Levy and Heald (2010; with permission from Elsevier). In vitro: nuclei assembled in *X. laevis* egg extract were incubated in LEE and visualized by NPC staining (mAb414). Complete details of the assay are described in the Materials and methods section. (B) Confocal z stacks (3-µm-thick sections) were acquired and maximum intensity projections are shown for representative nuclei. The control nuclei were treated with HI-LEE. *n* > 10 nuclei and 3 different extracts. (C) 3D surface plots are shown for the nuclei in B. (D) Nuclei treated with HI-LEE (control) and LEE were stained with mAb414. Nuclear surface area was calculated directly from confocal z stacks (blue bars), and nuclear surface area was then estimated for those same nuclei by measuring the cross-sectional area and multiplying by four (green bars). These values agreed within 3% (P > 0.7), which is consistent with these nuclei having roughly spherical geometry and validating our approach of estimating total NE surface area from the cross-sectional area. *n* = 20 nuclei each, error bars represent SD. (E) Nuclear shrinking data from 46 different extracts are shown. "Control Treated Nuclei" represent nuclei

nuclei become smaller when incubated in late embryo extract (LEE; stage 11.5–12 embryos). We reasoned that this activity, which we show is protein kinase C (PKC) dependent and acts on the nuclear lamina, might account for in vivo developmental nuclear scaling. Consistent with this idea, PKC activity and nuclear localization increase after the MBT, and altering PKC activity within interphase in the embryo affects nuclear size in vivo. We propose that up-regulation of cPKC-dependent nuclear shrinkage at the MBT balances nuclear import–mediated growth. This type of equilibrium balance model can explain why nuclei maintain a smaller, steady-state size after the MBT.

Results and discussion

A novel nuclear shrinking activity

To identify regulators of nuclear size in the post-MBT *Xenopus* embryo, we developed a novel in vitro nuclear resizing assay (Fig. 1 A). Nuclei were assembled de novo in interphase *X. laevis* egg extract, isolated by gentle centrifugation, and resuspended in cytoplasmic interphase extract prepared from stage 11.5–12 *X. laevis* embryos (LEE). After a 90-min incubation in LEE, nuclei exhibited a reduction in cross-sectional nuclear area of 29% ± 13% (mean ± SD; n = 46 different extracts). As confocal imaging showed that nuclei were roughly spherical before and after shrinking (Fig. 1, B–D), we extrapolated this reduction in nuclear size to being equivalent to 218 ± 41 µm^2 of NE. Between experiments, the reduction in nuclear surface area ranged from 8–63% and depended largely on the starting size of the de novo assembled nuclei, which varied greatly between egg extracts (Fig. 1 E). The most dramatic resizing occurred during the first 30 min of incubation, with nuclei subsequently reaching a smaller steady-state size (Fig. 1, F and G; and Video 1). Nuclei still excluded 150 kD dextran after incubation in LEE, which indicates that the NE remained intact (not depicted), and nuclear resizing was not dependent on filamentous actin or microtubules (Fig. S1 A).

To mitigate concerns that the observed reductions in nuclear size were caused by osmotic effects, we performed control reactions using LEE that had been pretreated at 56°C for 30 min before the addition of nuclei. This heat-inactivated (HI) extract was unable to resize nuclei (Fig. S1 B). Furthermore, specific small molecule and antibody inhibitors were identified that blocked nuclear shrinking when added to LEE (see the following section and Fig. 2). Nuclei resuspended in egg extract grew larger, showing that the shrinking activity is specific to LEE (Fig. S1 B). Compared with in vivo nuclear size, the magnitude of nuclear shrinking observed in our assay was comparable to the change in nuclear size between stage 10 and stage 14 post-MBT embryos (Fig. 1 H). Collectively, these data suggest that the activity responsible for nuclear resizing in our assay is physiologically relevant and may contribute to in vivo developmental nuclear scaling.

Nuclear shrinking is dependent on conventional PKC

To identify specific inhibitors of nuclear shrinking in our assay, we tested a panel of kinase inhibitors, adding inhibitors to LEE before resuspension of de novo assembled nuclei. Only chelerythrine, a PKC inhibitor (Herbert et al., 1990), prevented nuclear resizing (Fig. 2 A), which suggests that nuclear shrinking is PKC dependent. Chelerythrine had a specific effect in LEE, as addition of chelerythrine to egg extract did not alter the size of de novo assembled nuclei (Fig. 2 F), likely because PKC activity is low in egg extract (see the "PKC localization and activity" section and Fig. 5 D). Furthermore, consistent with PKC activity being heat sensitive (Hyatt et al., 1994), nuclei failed to resize in HI-LEE (Fig. S1 B). We also performed antibody inhibition experiments using an antibody that recognizes all PKC isoforms, hereafter referred to as the pan-PKC antibody. Nuclei failed to become smaller in LEE supplemented with this antibody (Fig. 2 B), more directly demonstrating the role of PKC in nuclear resizing.

PKCs are divided into four subfamilies distinguished by their cofactor dependence, and only conventional/classical PKCs (cPKC α, β, and γ) require both calcium and DAG for kinase activation (Edwards and Newton, 1997; Newton, 2003). To identify the PKC subfamily responsible for nuclear resizing, we tested cofactor dependence. Depleting LEE of DAG and/or calcium, using propranolol or EGTA, respectively (Fernández-Ulibarri et al., 2007), abrogated the nuclear resizing activity, and nuclear shrinking could be rescued by the addition of calcium to EGTA-treated LEE (Fig. 2 C). These data implicated the conventional PKC subfamily, but to show this more directly, we performed experiments with cPKC-specific antibodies and recombinant proteins. Supplementing LEE with an antibody that recognizes cPKC isozymes inhibited nuclear shrinking (Fig. 2 D), and the addition of constitutively active PKC β to chelerythrine-treated LEE rescued nuclear shrinking (Fig. 2 E). Furthermore, addition of constitutively active PKC β or a PKC activator (PMA) to egg extract reduced the growth of de novo assembled nuclei (Fig. 2 F). Collectively, these data support the idea that nuclear resizing is cPKC dependent.

---

incubated in either extract buffer or HI-LEE. Each bar shows the mean for >240 nuclei. Error bars represent SD. (F) Nuclei were assembled de novo in *X. laevis* egg extract supplemented with recombinant GFP-LB3 and incubated in LEE. Live time-lapse imaging was performed at 30-s intervals for 90 min (see Video 1). Figure panels show 10-min intervals of a representative shrinking nucleus. (G) De novo assembled nuclei were incubated in LEE or HI-LEE, fixed at 30-min intervals, and quantified. Error bars represent SD. One representative experiment out of eight is shown. (H) Box-and-whisker plots are shown comparing fold changes in nuclear surface area. The blue (control nuclei) and green (LEE-treated nuclei) bars show in vitro data from one representative experiment (n > 200 nuclei for each treatment), normalized to the mean size for the control treated nuclei. The purple (stage 10) and red (stage 14) bars are in vivo nuclear sizes (n > 140 nuclei for each stage), normalized to the mean size for stage 10 nuclei. Boxes represent 50% of the data and the thick black line represents the median. The upper and lower error bars represent the upper and lower quartile of the data, respectively. Bars: (A) 20 µm; (B and C) 5 µm; (F) 10 µm.

Figure 2. **Nuclear shrinking depends on conventional PKC activity.** The nuclear shrinking assay was performed as in Fig. 1. Nuclear size was normalized against the HI-LEE control in A–E. (A) Kinase inhibitors were added as follows: CDK-olomoucine (2 mM), PKA-KT 5720 (56 nM), Aurora kinase–ZM 447439 (20 µM), and PKC-chelerythrine (390 µM). $n = 6$ different extracts. (B) Pan-PKC or rabbit IgG control antibodies were added to LEE at 2.5 µg/ml. $n = 3$ different extracts. (C) Calcium depletion was accomplished by supplementing LEE with 1 mM EGTA. A 45-min EGTA treatment was rescued by the addition of 4 nM $CaCl_2$. DAG depletion was accomplished with 60 µM propranolol. $n = 4$ different extracts. (D) Inhibitory human PKC βI or rabbit IgG control antibodies were added to LEE at 2.5 µg/ml. $n = 2$ different extracts. (E) Where indicated, LEE was treated with chelerythrine (390 µM) for 45 min, then recombinant constitutively active PKC-β-ΔNPS (1 nM) was added followed by an additional 45-min incubation. $n = 2$ different extracts. (F) Nuclei were assembled de novo in *X. laevis* egg extract for 45 min. Chelerythrine (390 µM), constitutively active PKC-β-ΔNPS (1 nM), or PMA (1.6 µM) were then added, and nuclear expansion was allowed to progress for an additional 45 min. Nuclear size was normalized to the 45 min time point. $n = 5$ different extracts. ***, $P < 0.005$; **, $P < 0.01$; *, $P < 0.05$. Error bars represent SD.
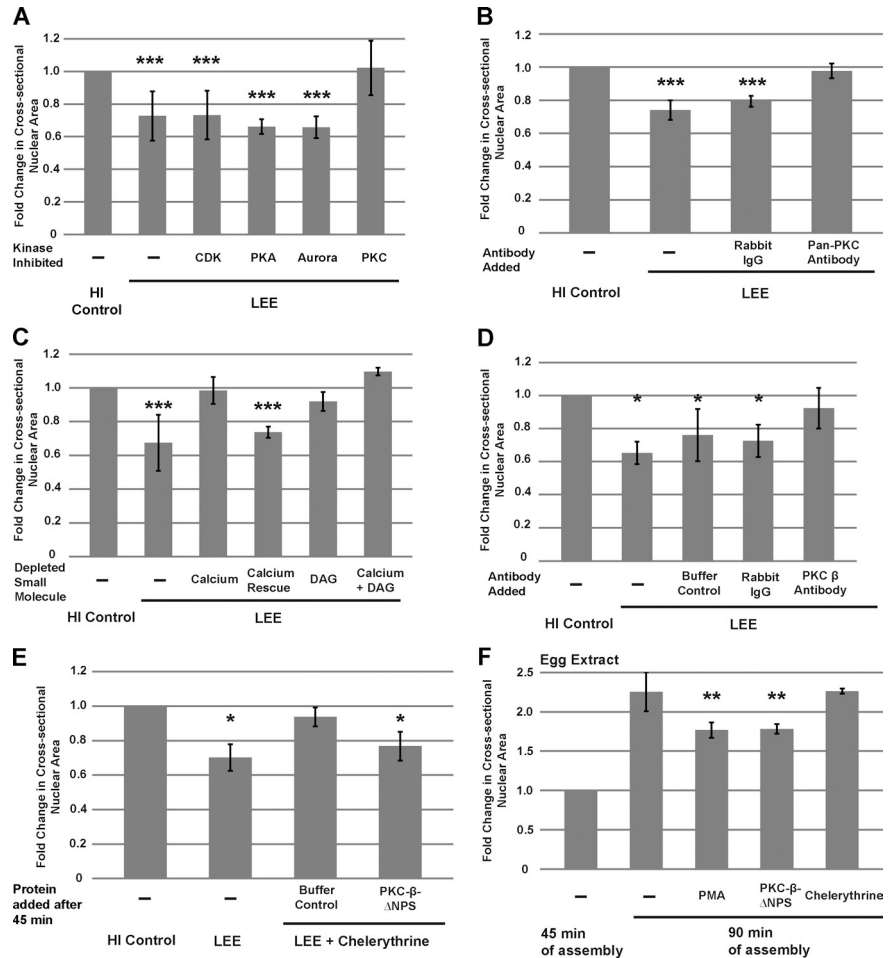
Nuclear lamins are downstream targets of cPKC signaling in nuclear shrinking

We reasoned that nuclear resizing must involve changes in components of the NE. We performed confocal imaging on the surface of nuclei to quantify nuclear pore complex (NPC) and nuclear lamin density at the NE, defined as staining intensity within a fixed defined region. Although NPC density increased after nuclear shrinking, total NPC staining per nucleus did not change (Fig. 1 B; Figs. 3, A and B; and Fig. S2, A and B), which suggests that NPCs are not being actively disassembled and that nuclear resizing is not mediated by large-scale dissolution of the NE, or by budding of NE vesicles or blebs containing NPCs.

The primary nuclear lamin present in de novo assembled nuclei is the egg-specific lamin B3 (LB3; Benavente et al., 1985). We measured LB3 density before and after nuclear shrinking by both LB3 immunofluorescence and using a GFP-LB3 fusion protein incorporated into de novo assembled nuclei. Nuclear lamina density at the NE did not change during shrinking, whereas total LB3 staining per nucleus became less, which indicates that nuclear resizing is accompanied by removal of nuclear lamins (Fig. 3, C and D; and Fig. S2, A and B). Furthermore, inhibiting nuclear resizing with the pan-PKC antibody concomitantly blocked removal of LB3 from the NE (Figs. 3 D and S2, A and B). These data show that some LB3 dissociates from the NE during shrinking, likely regulated by direct or indirect phosphorylation by cPKC.

Xenopus tropicalis nuclei and *X. laevis* somatic nuclei are sensitive to nuclear shrinking

To examine if PKC-dependent nuclear resizing was limited to *X. laevis* nuclei, we tested nuclei assembled in egg extract from the related species *X. tropicalis*. As with *X. laevis* nuclei, *X. tropicalis* nuclei became smaller when incubated in *X. laevis* LEE, and chelerythrine prevented nuclear shrinking (Fig. 4 A). To test nonembryonic nuclei whose nuclear lamina is composed of multiple lamin isoforms, we isolated nuclei from adult *X. laevis* liver and subjected these nuclei to the resizing assay (Sullivan et al., 1999). Somatic liver nuclei also became smaller (Fig. 4, B–D), despite starting out at a much smaller size than de novo assembled nuclei. Furthermore, chelerythrine prevented somatic nuclear shrinking (Fig. 4 C), and shrinking was accompanied by lamin B1 removal (Fig. 4 D). These data demonstrate that the cPKC-dependent nuclear resizing activity present in LEE can act on nuclei from the related species *X. tropicalis*, as well as on somatic nuclei that possess a different nuclear lamina composition.

## PKC localization and activity change over the course of development

To understand how PKC signaling might contribute to developmental nuclear scaling, we analyzed PKC levels and localization
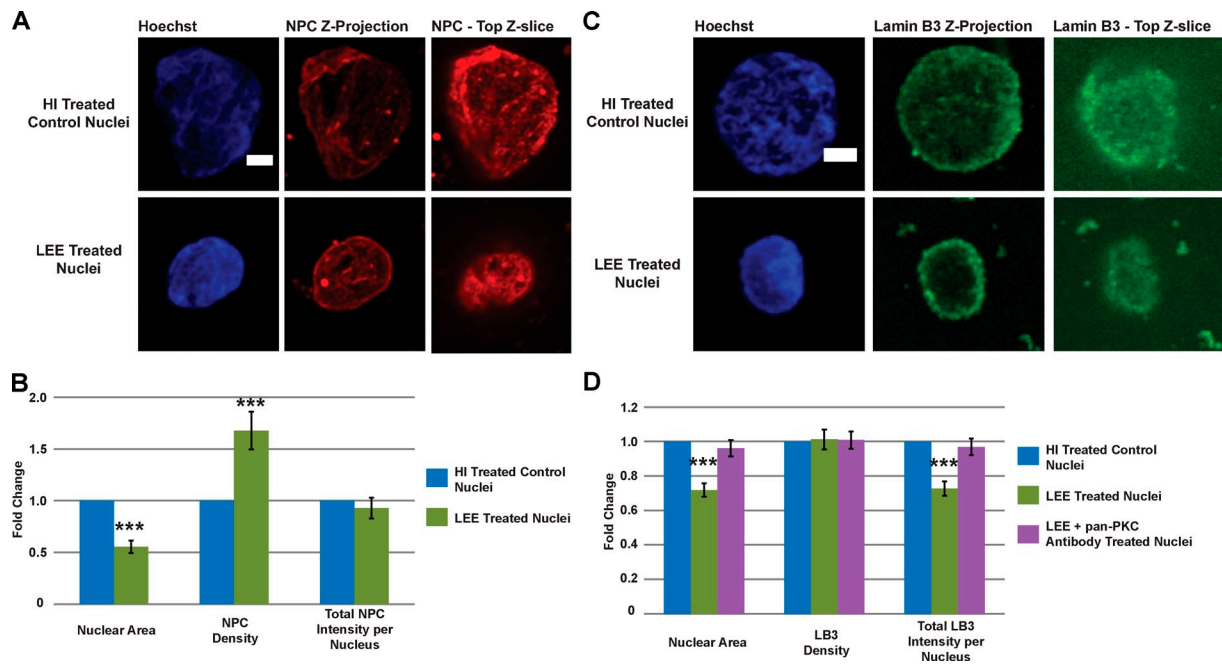
Figure 3. **Lamins are removed during nuclear shrinking in a PKC-dependent manner.** The nuclear shrinking assay was performed as in Fig. 1. Z-stack images were acquired by confocal microscopy. For intensity measurements, all images were acquired with the same exposure time. NPC and LB3 density at the NE were determined by quantifying staining intensity within a fixed defined area (20 μm²) for an individual z slice at the periphery of the nucleus. Total NE staining intensity per nucleus was estimated from the density measurement and total NE surface area. Shown in A and C are representative maximum-intensity projections and z slices at the periphery of nuclei used for intensity measurements. Bars, 5 μm. (A and B) NPCs were visualized with mAb414 (red). $n > 10$ different nuclei in two different extracts. (C and D) LB3 was visualized with an α-LB3 antibody (green). $n > 10$ different nuclei in two different extracts. ***, $P < 0.005$. Error bars represent SD.

over early development. We found that total PKC levels remain constant from stage 2 to stage 12 (Figs. 5 A and S1 C), which is consistent with *X. laevis* transcriptomics data (Yanai et al., 2011). PKC activation is frequently dependent on its membrane localization (Buchner, 2000; Newton, 2003), so we examined whether there was a change in PKC nuclear localization. Nuclei assembled in egg extract stained very weakly for cPKC, whereas endogenous stage 12 nuclei and nuclei subjected to

the in vitro shrinking assay exhibited a dramatic increase in nuclear cPKC localization (Fig. 5, B and C; and Fig. S2, C–F). Moreover, increased nuclear PKC localization correlated with higher levels of PKC activity in LEE compared with egg extract, detected using a PKC-specific peptide substrate (Fig. 5 D). Collectively, these data suggest that increased nuclear PKC localization and activity contribute to reduced nuclear size in post-MBT embryos.
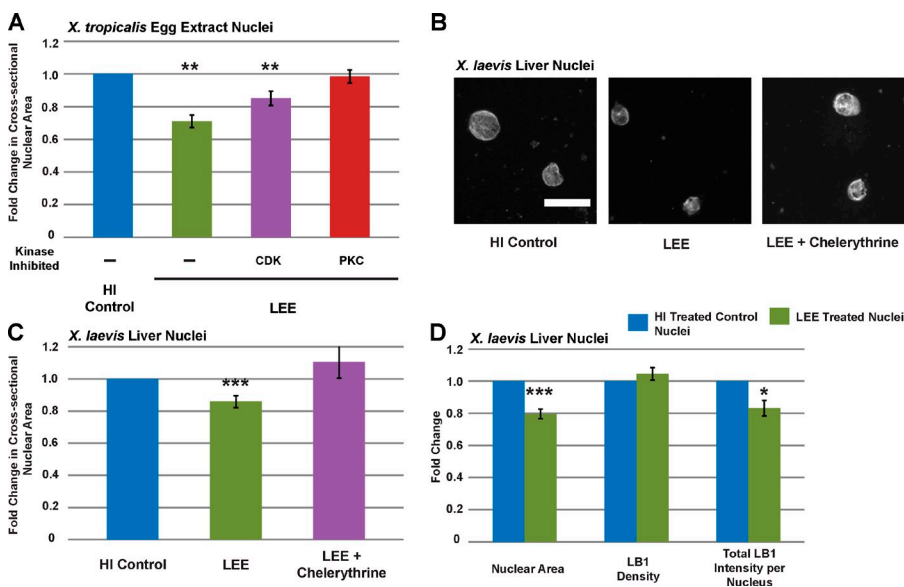
Figure 4. **Shrinking of *X. tropicalis* nuclei and somatic cell nuclei.** (A) Nuclei assembled de novo in *X. tropicalis* egg extract were subjected to the nuclear shrinking assay as described in Fig. 1. Kinase inhibitors were added to the same concentrations as in Fig. 2 A. (B and C) Nuclei were isolated from adult *X. laevis* liver, subjected to the nuclear shrinking assay, visualized with mAb414, and imaged by wide-field microscopy. $n = 4$ different liver nuclei preparations and extracts. Bar, 10 μm. (D) *X. laevis* liver nuclei treated with HI control extract or LEE were visualized by immunofluorescence using an antibody against lamin B1. Confocal imaging and quantification were performed as in Fig. 3. $n = 4$ different liver nuclei preparations and 3 extracts. ***, $P < 0.005$; **, $P < 0.01$; *, $P < 0.05$. Error bars represent SD.
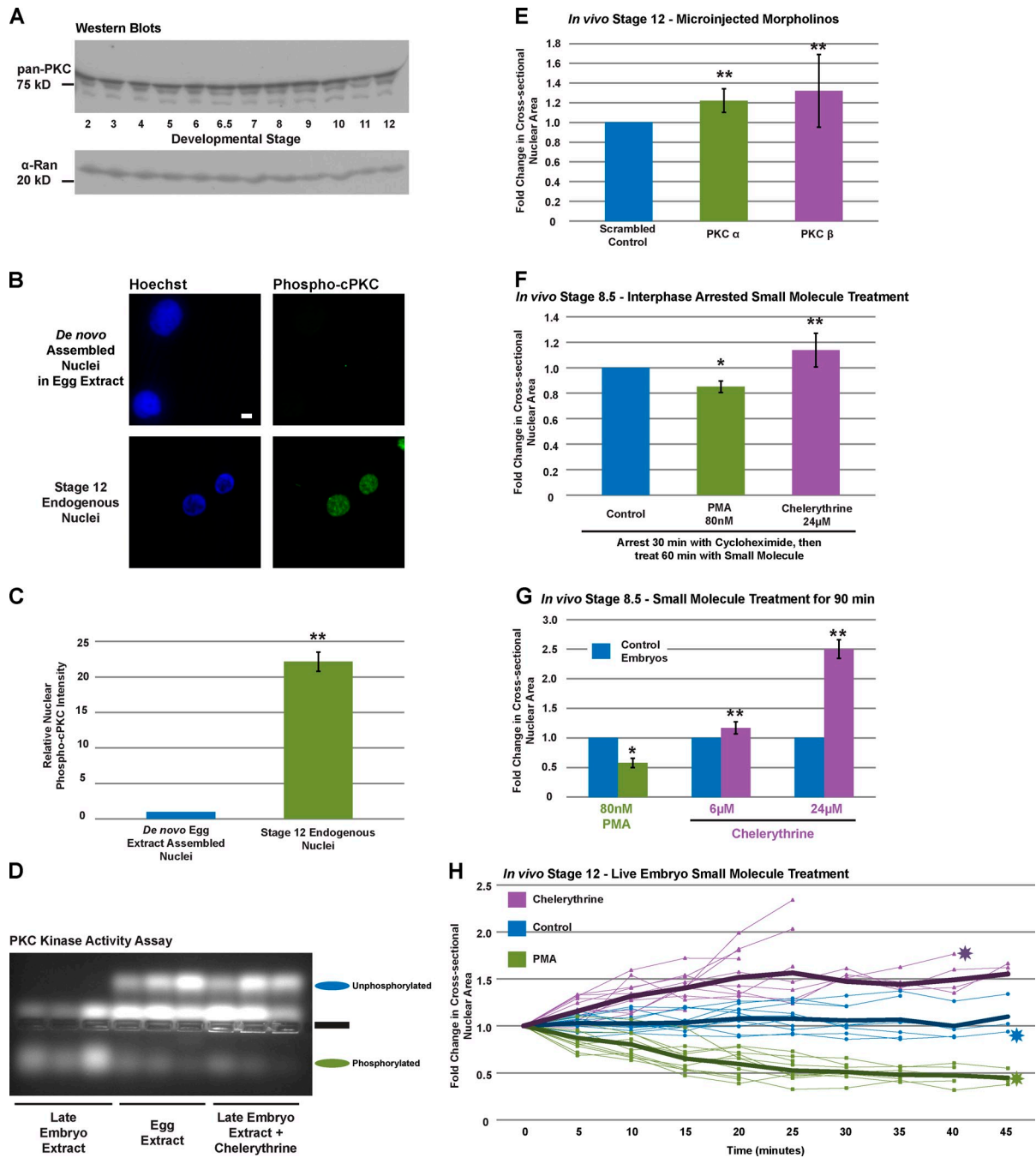
Figure 5. **PKC nuclear localization and activity increase during *X. laevis* development, and altering PKC activity in vivo affects nuclear size.** (A) Western blots of whole embryo lysates (0.6 embryo equivalents per lane) from stages 2–12 were probed with a pan-PKC or Ran antibody. $n = 2$ different sets of whole embryo preparations. One representative gel is shown. (B and C) Nuclei assembled de novo in egg extract and endogenous stage 12 nuclei were stained with a phospho-cPKC antibody (green). Confocal images were acquired, and PKC staining intensity was quantified as described in Fig. 3. $n = 2$ different extracts. Bar, 10 µm. (D) PKC activity was detected in extracts using a colorimetric PKC-specific peptide substrate (see Materials and methods). Unphosphorylated substrate migrates toward the anode (above the loading well) while phosphorylated substrate migrates toward the cathode (below the loading well). Results for three different egg extracts and LEEs are shown. Where indicated, chelerythrine was added at 390 µM. (E) One-cell embryos were microinjected with morpholinos against PKC α, PKC β, or a scrambled control and allowed to develop to stage 12. Nuclei isolated from embryos were visualized with mAb414 and quantified. $n = 3$ different fertilizations, with at least 20 embryos each. (F) Stage 8 embryos were arrested in interphase by incubating for 30 min in cycloheximide (0.5 mM), followed by a 60-min incubation with chelerythrine or PMA as indicated. Nuclei were quantified as in E. $n = 2$ different fertilizations, with at least 15 embryos each. (G) Stage 8 embryos were incubated for 90 min with chelerythrine or PMA as indicated. Nuclei were quantified as in E. $n = 2–3$ different fertilizations, with at least 20 embryos each. (H) Single-cell embryos were microinjected with GFP-NLS mRNA to visualize nuclei, and allowed to develop to stage 12. Embryos were treated with 24 µM chelerythrine or 80 nM PMA, as indicated, and confocal time-lapse images were acquired every minute on the surface of live embryos for 45 min (see Videos 2–10). For individual nuclei, cross-sectional nuclear area was quantified every 5 min and normalized to the size at t = 0. For each treatment condition, $n = 12$ nuclei from three movies of different embryos. Thicker lines denote averages for a given treatment, and stars refer to specific nuclei highlighted in Videos 2, 5, and 8. **, $P < 0.01$; *, $P < 0.05$. Error bars represent SD.

To test if the novel nuclear resizing activity we identified in vitro is also at work in vivo, we manipulated PKC activity in living *X. laevis* embryos. First, we microinjected single-cell embryos with morpholino oligonucleotides to reduce cPKC levels, and embryos were allowed to develop to stage 12. Compared with embryos injected with scrambled control morpholinos, embryos depleted of either cPKC α or β exhibited larger nuclei (Figs. 5 E and S2, G and H). Embryos injected with cPKC morpholinos appeared morphologically similar to control embryos at stage 12 and did not show obvious developmental delays.

As morpholino experiments require depletion of maternal protein pools over many hours, we performed complementary experiments in which PKC activity was acutely manipulated in live embryos using cell-permeable small molecules. Because our in vitro assay made exclusive use of interphase extracts, we wanted to know if altering PKC activity during interphase would have an effect on in vivo nuclear size. Stage 8 embryos were first arrested in late interphase with cycloheximide for 30 min (Lemaitre et al., 1998; Levy and Heald, 2010) and then treated with varying concentrations of a PKC activator (PMA) or inhibitor (chelerythrine) for 60 min (Herbert et al., 1990; Toker, 1998; Ron and Kazanietz, 1999). In interphase-arrested embryos, PKC activation reduced nuclear size, whereas PKC inhibition increased nuclear size (Fig. 5 F). Longer PMA and chelerythrine treatments had more dramatic effects, with PKC activation reducing nuclear surface area by up to $56 \pm 9\%$ (mean ± SD) and PKC inhibition increasing nuclear area by up to $150 \pm 10\%$ (Fig. 5 G).

To gain further support for the idea that PKC activity regulates nuclear size within interphase without using cycloheximide to arrest embryos, we performed live, time-lapse imaging of interphase nuclei in stage 12 embryos. Nuclei were visualized with a GFP-NLS construct microinjected at the one-cell stage, and dynamic changes in nuclear size were observed by confocal imaging on the surface of embryos. Although most nuclei in control embryos did not significantly change size over 45 min of imaging, nuclear growth was observed in embryos acutely treated with chelerythrine, and nuclear shrinkage occurred in embryos treated with PMA (Fig. 5 H and Videos 2–10). Importantly, we observed these size changes within interphase. In contrast to PKC signaling, altering nucleocytoplasmic transport in post-MBT embryos did not significantly affect nuclear size (Fig. S1 D). These in vivo data corroborate our in vitro results and suggest that up-regulated interphase cPKC activity contributes to nuclear size reductions during early *X. laevis* development.

Our findings represent a novel aspect of interphase nuclear dynamics that can account in part for developmental regulation of nuclear size in *Xenopus*. We propose that in vitro nuclear shrinking is mediated by the recruitment of cPKC to the nucleus, leading to phosphorylation of nuclear lamins that alters their residence time at the NE. PKC is known to phosphorylate lamins (Peter et al., 1990; Hocevar et al., 1993; Goss et al., 1994; Collas, 1999; Mall et al., 2012; Simon and Wilson, 2013). A tug-of-war relationship has been proposed between the NE and ER membrane systems (Anderson and Hetzer, 2008a,b; Webster et al., 2009), so we propose that loss of lamins from the NE may be compensated

for by retraction of NE membrane back into the ER, resulting in a reduction in NE surface area and maintenance of constant nuclear lamina density. In contrast to localized PKC activity required for budding of viruses and messenger RNPs (mRNPs) across the NE (Muranyi et al., 2002; Park and Baines, 2006; Leach and Roller, 2010; Milbradt et al., 2010; Speese et al., 2012; Porwal et al., 2013), our model posits that constitutive interphase nuclear PKC activity contributes to steady-state nuclear size regulation, and it has been demonstrated that lamins are phosphorylated in interphase (Hennekes et al., 1993; Kill and Hutchison, 1995; Hatch and Hetzer, 2014; Kochin et al., 2014). In fact, it seems reasonable that nuclear egress of viral capsids and mRNPs may be mediated by local up-regulation of a constitutive, basal PKC activity already acting at the NE.

One model for how in vitro nuclear shrinking might relate to in vivo developmental nuclear scaling is that rising PKC activity limits NE expansion as development proceeds, which is consistent with lamin import being inhibited by PKC phosphorylation (Hennekes et al., 1993). However, this model predicts that increasing PKC activity within interphase should slow nuclear growth or have no effect on nuclear size, not cause a reduction in nuclear size, as we observe both in vivo with PMA treatment (Fig. 5, F–H) and in vitro (Figs. 1–4). We believe our data are more consistent with an equilibrium balance model involving balancing rates of nuclear assembly and disassembly (Marshall, 2002). We propose that our newly identified in vitro nuclear shrinking activity represents the disassembly activity needed to describe an equilibrium balance model of nuclear size regulation. The simplest model is one where nuclear expansion, mediated by nuclear import, is balanced by a contraction rate that is proportional to the size of the nucleus. A steady-state size is achieved when the growth rate matches the shrinking rate (Fig. S3).

Previous work has shown that in the early embryo before the MBT, limiting import appears to be a predominant determinant of nuclear size (Levy and Heald, 2010). By our equilibrium balance model, pre-MBT nuclei expand continuously because nuclear cPKC activity is low. After the MBT, increased cPKC activity becomes an important regulator of interphase nuclear size by up-regulating nuclear shrinkage activity that balances nuclear import–mediated growth. Furthermore, this growth-balancing activity can account for why nuclei in the post-MBT embryo reach a steady-state size and scale smaller.

In cancer cells, PKC signaling and nuclear size are both routinely deregulated and used independently in diagnosis and prognosis (Buchner, 2000; Zink et al., 2004; Mochly-Rosen et al., 2012; Edens et al., 2013; Jevtić and Levy, 2014; Jevtić et al., 2014). Our new insights into mechanisms of nuclear size regulation will help to elucidate the functional significance of nuclear size and could reveal novel relationships between deregulated PKC signaling and increased nuclear size in cancer cells.

Materials and methods

X. laevis egg extract and nuclear assembly

X. laevis and *X. tropicalis* metaphase-arrested egg extracts (Maresca and Heald, 2006; Brown et al., 2007; Edens and Levy, 2014) and *X. laevis* sperm (Murray, 1991) were prepared as described previously. In brief, eggs were dejellied, washed, packed, and subjected to a crushing centrifugation spin. Cytoplasmic extract was collected and supplemented with

protease inhibitors, cytochalasin D, and an energy mix. A 100 µl nuclear assembly reaction was initiated by the addition of 1.5 µl of 35.5 mM cycloheximide, 6 µl of 10 mM CaCl₂, and 0.7 µl of 100× demembranated *X. laevis* sperm, mixed by gentle inversion, and incubated at 16–21°C for 90 min, mixing every 15 min. Nuclear assembly was monitored by Hoechst staining. Nuclei were stored in egg extract at −80°C. All *Xenopus* procedures and studies were conducted in compliance with the US Department of Health and Human Services Guide for the Care and Use of Laboratory Animals. Protocols were approved by the University of Wyoming Institutional Animal Care and Use Committee (Assurance #A-3216-01).

X. laevis embryo extract

X. laevis embryos were generated by in vitro fertilization as described previously (Sive et al., 2000; Grammer et al., 2005). In brief, freshly laid eggs were incubated with crushed testes for 5–10 min, flooded with culture medium (1/3× MMR = 33 mM NaCl, 0.7 mM KCl, 0.3 mM MgSO₄, 0.7 mM CaCl₂, and 1.7 mM Hepes, pH 7.4), and dejellied in 2–3% cysteine, pH 7.9. Staged embryos (stage 11.5–12 for LEE) were incubated in 0.5 mM cycloheximide in 1/3× MMR at room temperature for 60 min to arrest embryos in late interphase. Embryos (between 30 and 500) were transferred to a microcentrifuge tube and washed three times with 1 ml ELB (250 mM sucrose, 50 mM potassium chloride, 2.5 mM magnesium chloride, and 10 mM Hepes, pH 7.8) including 1:1,000 volume of LPC (10 mg/ml each of leupeptin, pepstatin, and chymostatin). Embryos were then washed in 500 µl of the same buffer including 0.1 mg/ml each of cytochalasin D and cycloheximide, and centrifuged at 200 *g* for 1 min. Excess buffer was removed, and embryos were crushed with a pestle followed by centrifugation in a swinging bucket rotor at 10,000 *g* for 10 min at 16°C. The cytoplasmic layer was collected and supplemented with 1:50 volume of 50× energy mix (190 mM creatine phosphate disodium, 25 mM ATP disodium salt, 25 mM magnesium chloride), 1:100 volume of 35.5 mM cycloheximide, 1:500 volume of 19.7 mM cytochalasin D, and 1:1,000 volume of LPC. To remove embryonic nuclei, the extract was diluted 1:1 with ELB containing 1:50 volume of 50× energy mix, 1:100 volume of 35.5 mM cycloheximide, 1:500 volume of 19.7 mM cytochalasin D, and 1:1,000 volume of LPC, then centrifuged in a swinging bucket rotor at 17,000 *g* for 15 min at 16°C. The cytoplasmic layer was collected (LEE) and stored at −80°C. Heat inactivation was achieved by incubating 30–100 µl of extract at 56°C for 30 min.

Nuclear shrinking assay

De novo nuclei assembled in *Xenopus* egg extract (25 µl) were diluted in 1 ml of ELB. Nuclei were pelleted at 1,600 *g* in a tabletop centrifuge for 3 min at room temperature. Diluted egg extract was discarded. Nuclei were resuspended in 25 µl of LEE, HI-LEE, or buffer (ELB containing 1:50 volume of 50× energy mix, 1:100 volume of 35.5 mM cycloheximide, 1:500 volume of 19.7 mM cytochalasin D, and 1:1,000 volume of LPC). Where indicated, LEE was immediately supplemented with small molecules, recombinant proteins, or antibodies. Reactions were gently mixed and incubated at room temperature for 90 min. Nuclei were fixed and visualized as described under "Immunofluorescence and microscopy."

Small molecules, antibodies, and recombinant proteins

Small molecules. Chelerythrine chloride (C2932), PMA (P8139), KT 5720 (PKA inhibitor; K3761), and olomoucine (O0886) were purchased from Sigma-Aldrich and reconstituted in water, DMSO, methanol, or DMSO, respectively. ZM 447439 (Aurora Kinase Inhibitor VI; 189410) was purchased from EMD Millipore and reconstituted in DMSO. Working concentrations were selected based on the literature (Collas et al., 1997; Gadea and Ruderman, 2005; Lane et al., 2010). Concentrations used in vitro were olomoucine (2 mM), chelerythrine (390 µM), KT 5720 (56 nM), and ZM 447439 (20 µM). Note that the chelerythrine concentration used in vitro in extract was much higher than the concentrations used for in vivo treatment of embryos. It is common that higher concentrations of small molecule inhibitors are required in *Xenopus* extract, compared with in vivo, to have a maximal effect.

Antibodies. The pan-PKC antibody (sc-10800; Santa Cruz Biotechnology, Inc.) is a rabbit polyclonal antibody used at 1:50 for immunofluorescence and 1:1,000 for Western blots. For antibody inhibition experiments (Figs. 2 B and 3 D), the antibody was dialyzed into ELB and supplemented into LEE at 2.5 µg/ml. The human PKC-βI antibody (GTX113252; Genetex) is a rabbit polyclonal antibody that was dialyzed into ELB and used at 2.5 µg/ml for antibody inhibition experiments (Fig. 2 D); the epitope recognized by this antibody is 80% identical to *X. laevis* PKC α and 92% identical to *X. laevis* PKC β, and has little similarity to PKC isozymes outside

the cPKC subfamily. A rabbit antibody that recognizes phospho-PKC α/β (bs-3333R; Bioss Inc.) was used at a dilution of 1:100 for immunofluorescence (Fig. 5, B and C). Rabbit IgG (Sigma-Aldrich) and antibodies against LB3 (rabbit antibody raised against amino acids 460–559 of *X. tropicalis* LB3) and Ran (mouse antibody from BD) were used as described previously (Levy and Heald, 2010). The LB3 antibody was used at a dilution of 1:100 for immunofluorescence. The lamin B1 antibody (ab16048; Abcam) is a rabbit polyclonal antibody used at 1:500 for immunofluorescence. Mouse mAb414 (Abcam) was used at 1:1,000 for immunofluorescence. Secondary antibodies were used at 1:1,000 for immunofluorescence and included DyLight 488 and DyLight 594 conjugated anti–mouse and anti–rabbit IgG antibodies (Jackson ImmunoResearch Laboratories, Inc.).

Recombinant proteins. Recombinant GFP-LB3 was purified as described previously (Levy and Heald, 2010). In brief, 6×His-GFP-LB3 was expressed in bacteria, cells were lysed, and inclusion bodies were solubilized under denaturing conditions. GFP-LB3 was refolded by dialysis, purified on Ni-NTA resin (QIAGEN), and dialyzed into LB3 storage buffer (10 mM Hepes, 300 mM KCl, 50 mM sucrose, and 5% glycerol, pH 7.8) at ∼1 mg/ml. To purify PKC, we obtained plasmid 16379 from Addgene. This is a mammalian expression vector (pHACE, C-terminal HA tag) with rat PKC β1 lacking the N-terminal pseudosubstrate domain (amino acids 1–29) cloned at EcoRI. The expressed protein, termed PKC β1 dNPS, is constitutively active (Soh and Weinstein, 2003). We subcloned the PKC β1 dNPS coding sequence into pGEX-4T-1 at BamHI to generate an N-terminal GST fusion (pDL51 = PKC β1 dNPS pGEX-4T-1). Plasmid pDL51 was transformed into BL21-CodonPlus(DE3)-RIL cells (Agilent Technologies). 1 liter LB/ampicillin/chloramphenicol cultures were grown at 37°C to OD₆₀₀ₙₘ ∼0.5. Recombinant protein expression was induced with 1 mM IPTG at 37°C for ∼4 h. Cells were harvested and lysed in 15 ml of PKC extraction buffer (50 mM Hepes, pH 7.8, 150 mM NaCl, 0.1% Tween 20, 1 mM EDTA, 2.5 mM EGTA, and 10% glycerol) plus protease inhibitors (1:1,000 volume of LPC, 1 mM PMSF, and Sigmafast protease inhibitor cocktail), phosphatase inhibitors (1 mM NaF and 0.1 mM Na₃VO₄), and ∼100 µM lysozyme, followed by sonication. After centrifugation to remove cell debris, clarified lysate was incubated with 300 µl glutathione agarose (Thermo Fisher Scientific) at 4°C for ∼1 h. Resin was washed three times with 5 ml PKC extraction buffer, and bound protein was eluted with 250 mM sucrose, 150 mM KCl, 2.5 mM MgCl₂, 50 mM Hepes, 10% glycerol, 10 mM reduced glutathione, and 10 mM DTT, pH 7.7. Eluate was dialyzed (3,500 molecular weight cutoff) into 250 mM sucrose, 50 mM KCl, 2.5 mM MgCl₂, 10 mM Hepes, pH 7.8, and 10% glycerol. Protein aliquots were flash-frozen in liquid nitrogen and stored at −80°C. The protein concentration was ∼20 nM and the purified protein was recognized in Western blots using the pan-PKC antibody. Purified PKC β1 dNPS was added to extract at a concentration of ∼1 nM (Fig. 2, E and F).

Immunofluorescence and microscopy

Nuclei in 25-µl reactions were fixed with 500 µl ELB, 15% glycerol, and 2.6% paraformaldehyde for 15 min with constant rotation at room temperature. Fixed nuclei were spun down onto round coverslips (12 mm diameter, No. 1.5) through 5 ml of nucleus cushion buffer (100 mM KCl, 1 mM MgCl₂, 100 µM CaCl₂, 0.2 M sucrose, and 25% glycerol) in a swinging bucket rotor at 1,000 *g* for 15 min at 16°C. Nuclei were post-fixed in cold methanol for 5 min, rehydrated in PBS, 3% BSA, 0.1% NP-40 for 20 s, and blocked in PBS–3% BSA overnight at 4°C. Nuclei were incubated for 60 min at room temperature with primary antibody, washed, incubated for 60 min with secondary antibody, washed, and stained with 5 µg/ml Hoechst for 5 min (antibodies were diluted in PBS—3% BSA as indicated in the "Antibodies" section). Coverslips were mounted on slides with Vectashield mounting medium (Vector Laboratories) and sealed with nail polish.

For wide-field microscopy, nuclei were visualized with a fluorescence microscope (BX51; Olympus) using the following objectives: UPLFLN 20× (NA 0.50, air; Olympus), UPLFLN 40× (NA 0.75, air; Olympus), and UPLANAPO 60× (NA 1.20, water; Olympus). Images were acquired with a QIClick Digital charge-coupled device (CCD) camera, mono, 12-bit (model QIClick-F-M-12) using cellSens software (Olympus). Images for measuring fluorescence staining intensity were acquired using the same exposure times. Total fluorescence intensity and cross-sectional nuclear area were measured from the original thresholded images using MetaMorph software (Molecular Devices). For publication, images were cropped and pseudocolored using ImageJ, but were otherwise unaltered.

Confocal imaging was performed on a spinning-disk confocal microscope based on a microscope stand (IX71; Olympus) equipped with a five line LMM5 laser launch (Spectral Applied Research) and switchable two-fiber output to facilitate imaging through either a spinning-disk head

(CSU-X1; Yokogawa Electric Corporation) or a total internal reflection fluorescence illuminator. Confocal images were acquired with an EM-CCD camera (ImagEM; Hamamatsu Photonics). Z-axis focus was controlled using a piezo Pi-Foc (Physik Instrumente), and multiposition imaging was achieved using a motorized Ludl stage. Objectives used were an UPLSAPO 20× (NA 0.85, oil) and APON 60× (NA 1.49, oil; both from Olympus). Image acquisition and all system components were controlled using MetaMorph software, and images for measuring fluorescence staining intensity were acquired using the same exposure times. 3-µm-thick z slices were collected for individual nuclei for total nuclear surface area calculations (ImageJ; Fig. 1, C and D). ImageJ was used to generate 3D surface plots and maximum intensity projections. The outermost image on the surface of the NE was used to measure the staining intensity per unit area (within a 20-µm^2 region) of lamins, NPCs, and PKC (MetaMorph software; Figs. 3–5). To calculate total staining intensity per nucleus, the density measurement was corrected for total nuclear surface area.

All imaging was performed at room temperature (∼20°C). Vectashield mounting medium (Vector Laboratories) was used for slides, and live embryo imaging was performed in 1/3× MMR. Fluorochromes included DyLight 488– and DyLight 594–conjugated anti–mouse and anti–rabbit IgG antibodies (Jackson ImmunoResearch Laboratories, Inc.), Hoechst (Sigma-Aldrich), and GFP.

PKC kinase activity assay
The PKC kinase assay (Fig. 5 D) was performed as described in the Promega PepTag Assay for Non-Radioactive Detection of Protein Kinase C protocol (V5330). In brief, reactions were prepared by combining 5 µl of Peptag PKC Reaction 5× buffer, 5 µl of PKC Activator 5× Solution, 5 µl of Peptag C1 peptide, 0.5 µl of 200 mM PMSF, and 9 µl of PKC source (egg extract, LEE, or LEE supplemented with cherlerythrine). The protein concentrations of egg and stage 12 embryo extracts were normalized based on Bradford assays, and 225 ng of total extract protein was added to each reaction as the source of PKC. After a 30-min incubation at 30°C, samples were boiled for 10 min, and 1 µl of 80% glycerol was added to each reaction. Reactions were loaded onto a 0.8% agarose gel prepared in TAE (40 mM Tris, 20 mM acetic acid, and 1 mM EDTA). The gel was run at 100 V for ∼40 min, and the PKC substrate was visualized with UV irradiation.

X. laevis liver nuclei isolation
Liver tissue isolated from adult X. laevis females was washed in cold PBS and immediately subjected to the soft tissue protocol in the Nuclei Enrichment kit for Tissue (89841; Thermo Fisher Scientific). At the end of the procedure, nuclei from one liver were collected in a total volume of 2 ml and the concentration of purified nuclei was estimated by Hoechst staining. 100 µl of liver nuclei was diluted in 1 ml of ELB, isolated by gentle centrifugation at 1,600 g for 3 min, and subjected to the nuclear shrinking assay.

Western blots
For each developmental stage, 20 X. laevis embryos were gently packed by centrifugation at 200 g for 1 min, all culture medium was removed, and embryos were resuspended in 400 µl of 20 mM Tris, pH 8.0, 100 mM NaCl, 1 mM EDTA, 0.5% Triton X-100, 10% glycerol, 0.5% SDS, and 1:1,000 volume of LPC. After a 10-min room temperature incubation, embryos were crushed with a pestle and centrifuged in a swinging bucket rotor at 13,000 g for 20 min at 4°C. The cleared supernatant was collected, supplemented with 1× SDS-PAGE sample buffer, boiled for 5 min, and stored at −80°C. 15 µl of each sample was separated on a 10% SDS-PAGE gel. Proteins were transferred to PVDF membrane using a semidry blotting apparatus (Bio-Rad Laboratories). The membrane was blocked in 5% milk in PBS–0.1% Tween 20 for 60 min, incubated with a 1:1,000 dilution of pan-PKC antibody overnight at 4°C, and then incubated with a 1:15,000 dilution of goat anti–rabbit HRP secondary antibody (31460; Thermo Fisher Scientific) for 60 min at room temperature. HRP detection was with ECL reagents (Thermo Fisher Scientific) and GeneMate Blue Autoradiography film. Membranes were subsequently stripped and reprobed with an antibody against Ran as described previously (Levy and Heald, 2010). Band quantification was performed using ImageJ, and PKC band intensities were normalized against Ran.

X. laevis embryo treatments in vivo
For small molecule treatment experiments, stage 8 X. laevis embryos were incubated for 90 min in culture medium supplemented with small molecules PMA (80 nM) or cherlerythrine (6 µM and 24 µM; Fig. 5 G). As noted in the "Small molecules, antibodies, and recombinant proteins" section, lower concentrations of cherlerythrine were used for these in vivo experiments as compared with the in vitro nuclear shrinking assay. In some cases, embryos were pretreated with cycloheximide (0.5 mM) for 30 min to arrest those embryos in late interphase (Lemaitre et al., 1998; Levy and Heald, 2010) and, subsequently, interphase-arrested embryos were treated with cherlerythrine or PMA for an additional 60 min (Fig. 5 F). For morpholino experiments, one-cell X. laevis embryos were microinjected with 10 nl of 1 mM morpholino oligonucleotides (Gene Tools, LLC) using a Picospritzer III and allowed to develop to stage 12. Morpholino sequences: PKC α, 5'-CGTTGTGCTGGAAGACATCAGCCAT-3'; PKC β, 5'-ACATGCTCC-GGTCGCAGTGTGTCCA-3'; scrambled standard control, 5'-CCTCT-TACCTCAgTTACAATTTATA-3'. To quantify nuclear size, embryo extract was prepared using 15–50 embryos (see "X. laevis embryo extract"), except the cycloheximide treatment was omitted, unless otherwise noted, and nuclei were not removed. After the crushing spin at 10,000 g for 10 min at 16°C, nuclei in the cytoplasmic extract were fixed and visualized (see "Immunofluorescence and microscopy").

For live embryo imaging, the SV40 NLS fused to GFP was cloned from pMD49 (a gift from M. Dasso, National Institutes of Health/National Institute of Child Health and Human Development, Bethesda, MD) into pCS2+ (generating pDL20), and mRNA was expressed and purified for the SP6 promoter using the mMessage mMachine kit (Ambion). Single-cell embryos were microinjected with 10 nl of 50 ng/µl GFP-NLS mRNA. Once injected embryos reached stage 12, they were placed in a glass-bottom Petri dish in 1/3× MMR only or 1/3× MMR supplemented with cherlerythrine (24 µM) or PMA (80 nM). Time-lapse imaging of nuclei containing GFP-NLS was performed on the surface of embryos by confocal microscopy (see "Immunofluorescence and microscopy"). Images were acquired every minute for 45 min. For nuclear size quantification, nuclei that were in focus and in interphase for the duration of a given movie were selected, and nuclear cross-sectional area was measured at each time point using ImageJ. At least four nuclei from each movie were quantified.

Statistics
Unless otherwise noted, nuclear cross-sectional areas were measured from thresholded images in MetaMorph (Molecular Devices). For each coverslip, at least 110, and usually >240, nuclei were quantified, and areas were averaged. Unless otherwise noted, nuclear area measurements were normalized to controls. Averaging and statistical analysis were performed for independently repeated experiments. Two-tailed Student's t tests assuming equal variances were performed in Excel (Microsoft) to evaluate statistical significance. The p-values, number of independent experiments, and error bars are denoted in the figure legends. The box-and-whisker plot (Fig. 1 H) was calculated and constructed in R language.

Online supplemental material
Fig. S1 shows that nuclear shrinking is not dependent on microtubules or filamentous actin, that nuclear shrinking depends on a heat-sensitive activity in embryo extracts, that PKC protein levels remain constant during early X. laevis development, and that blocking nuclear export does not affect nuclear size in vivo in the early embryo. Fig. S2 shows NPC and LB3 quantification from wide-field microscopy images, and shows that nuclear PKC staining increases upon nuclear shrinking, that nuclear PKC staining is greater in stage 12 nuclei than in de novo assembled nuclei, that PKC morpholino injections deplete PKC levels, and that PKC depletion by morpholino injection increases nuclear size in embryos. Fig. S3 depicts the equilibrium balance model of steady-state nuclear size regulation. Video 1 shows time-lapse imaging of nuclei resizing in the nuclear shrinking assay. Videos 2–4 show time-lapse imaging of control stage 12 embryos. Videos 5–7 show time-lapse imaging of cherlerythrine-treated stage 12 embryos. Videos 8–10 show time-lapse imaging of PMA-treated stage 12 embryos. Online supplemental material is available at http://www.jcb.org/cgi/content/full/jcb.201406004/DC1.

References

Anderson, D.J., and M.W. Hetzer. 2008a. Reshaping of the endoplasmic reticulum limits the rate for nuclear envelope formation. *J. Cell Biol.* 182:911–924. http://dx.doi.org/10.1083/jcb.200805140

Anderson, D.J., and M.W. Hetzer. 2008b. The life cycle of the metazoan nuclear envelope. *Curr. Opin. Cell Biol.* 20:386–392. http://dx.doi.org/10.1016/j.ceb.2008.03.016

Benavente, R., G. Krohne, and W.W. Franke. 1985. Cell type-specific expression of nuclear lamina proteins during development of *Xenopus laevis*. *Cell.* 41:177–190. http://dx.doi.org/10.1016/0092-8674(85)90072-8

Blom, J.H., F.J. Ten Kate, F.H. Schroeder, and R.O. van der Heul. 1990. Morphometrically estimated variation in nuclear size. *Urol. Res.* 18:93–99. http://dx.doi.org/10.1007/BF00302467

Brown, K.S., M.D. Blower, T.J. Maresca, T.C. Grammer, R.M. Harland, and R. Heald. 2007. *Xenopus tropicalis* egg extracts provide insight into scaling of the mitotic spindle. *J. Cell Biol.* 176:765–770. http://dx.doi.org/10.1083/jcb.200610043

Buchner, K. 2000. The role of protein kinase C in the regulation of cell growth and in signalling to the cell nucleus. *J. Cancer Res. Clin. Oncol.* 126:1–11. http://dx.doi.org/10.1007/PL00008458

Chan, R.C., and D.I. Forbes. 2006. In vitro study of nuclear assembly and nuclear import using *Xenopus* egg extracts. *Methods Mol. Biol.* 322:289–300. http://dx.doi.org/10.1007/978-1-59745-000-3_20

Collas, P. 1999. Sequential PKC- and Cdc2-mediated phosphorylation events elicit zebrafish nuclear envelope disassembly. *J. Cell Sci.* 112:977–987.

Collas, P., L. Thompson, A.P. Fields, D.L. Poccia, and J.-C. Courvalin. 1997. Protein kinase C-mediated interphase lamin B phosphorylation and solubilization. *J. Biol. Chem.* 272:21274–21280. http://dx.doi.org/10.1074/jbc.272.34.21274

Dekker, J., M.A. Marti-Renom, and L.A. Mirny. 2013. Exploring the three-dimensional organization of genomes: interpreting chromatin interaction data. *Nat. Rev. Genet.* 14:390–403. http://dx.doi.org/10.1038/nrg3454

Dey, P. 2010. Cancer nucleus: morphology and beyond. *Diagn. Cytopathol.* 38:382–390.

Edens, L.J., and D.L. Levy. 2014. Size scaling of subcellular organelles and structures in *Xenopus laevis* and *Xenopus tropicalis*. *In* Xenopus Development. M. Kloc, and J.Z. Kubiak, editors. John Wiley & Sons, Inc., Hoboken, NJ. 325–345. http://dx.doi.org/10.1002/9781118492833.ch17

Edens, L.J., K.H. White, P. Jevtic, X. Li, and D.L. Levy. 2013. Nuclear size regulation: from single cells to development and disease. *Trends Cell Biol.* 23:151–159. http://dx.doi.org/10.1016/j.tcb.2012.11.004

Edwards, A.S., and A.C. Newton. 1997. Regulation of protein kinase C βII by its C2 domain. *Biochemistry*. 36:15615–15623. http://dx.doi.org/10.1021/bi9718752

Fernández-Ulibarri, I., M. Vilella, F. Lázaro-Diéguez, E. Sarri, S.E. Martínez, N. Jiménez, E. Claro, I. Mérida, K.N. Burger, and G. Egea. 2007. Diacylglycerol is required for the formation of COPI vesicles in the Golgi-to-ER transport pathway. *Mol. Biol. Cell*. 18:3250–3263. http://dx.doi.org/10.1091/mbc.E07-04-0334

Gadea, B.B., and J.V. Ruderman. 2005. Aurora kinase inhibitor ZM447439 blocks chromosome-induced spindle assembly, the completion of chromosome condensation, and the establishment of the spindle integrity checkpoint in *Xenopus* egg extracts. *Mol. Biol. Cell*. 16:1305–1318. http://dx.doi.org/10.1091/mbc.E04-10-0891

Gerhart, J.C. 1980. Mechanisms regulating pattern formation in the amphibian egg and early embryo. *In* Biological Regulation and Development Vol. 2. R.F. Goldberger, editor. Plenum Press, New York. 133–316.

Goss, V.L., B.A. Hocevar, L.J. Thompson, C.A. Stratton, D.J. Burns, and A.P. Fields. 1994. Identification of nuclear β_{II} protein kinase C as a mitotic lamin kinase. *J. Biol. Chem.* 269:19074–19080.

Grammer, T.C., M.K. Khokha, M.A. Lane, K. Lam, and R.M. Harland. 2005. Identification of mutants in inbred *Xenopus tropicalis*. *Mech. Dev.* 122:263–272. http://dx.doi.org/10.1016/j.mod.2004.11.003

Hatch, E., and M. Hetzer. 2014. Breaching the nuclear envelope in development and disease. *J. Cell Biol.* 205:133–141. http://dx.doi.org/10.1083/jcb.201402003

Hennekes, H., M. Peter, K. Weber, and E.A. Nigg. 1993. Phosphorylation on protein kinase C sites inhibits nuclear import of lamin B2. *J. Cell Biol.* 120:1293–1304. http://dx.doi.org/10.1083/jcb.120.6.1293

Herbert, J.M., J.M. Augereau, J. Gleye, and J.P. Maffrand. 1990. Chelerythrine is a potent and specific inhibitor of protein kinase C. *Biochem. Biophys. Res. Commun.* 172:993–999. http://dx.doi.org/10.1016/0006-291X(90)91544-3

Hocevar, B.A., D.J. Burns, and A.P. Fields. 1993. Identification of protein kinase C (PKC) phosphorylation sites on human lamin B. Potential role of PKC in nuclear lamina structural dynamics. *J. Biol. Chem.* 268:7545–7552.

Hyatt, S.L., L. Liao, A.C. Nairn, and S. Jaken. 1994. Correlation between protein kinase C binding proteins and substrates in REF52 cells. *Cell Growth Differ.* 5:495–502.

Jevtić, P., and D.L. Levy. 2014. Mechanisms of nuclear size regulation in model systems and cancer. *Adv. Exp. Med. Biol.* 773:537–569. http://dx.doi.org/10.1007/978-1-4899-8032-8_25

Jevtić, P., L.J. Edens, L.D. Vuković, and D.L. Levy. 2014. Sizing and shaping the nucleus: mechanisms and significance. *Curr. Opin. Cell Biol.* 28C:16–27. http://dx.doi.org/10.1016/j.ceb.2014.01.003

Kill, I.R., and C.J. Hutchison. 1995. S-phase phosphorylation of lamin B2. *FEBS Lett.* 377:26–30. http://dx.doi.org/10.1016/0014-5793(95)01302-4

Kochin, V., T. Shimi, E. Torvaldson, S.A. Adam, A. Goldman, C.G. Pack, J. Melo-Cardenas, S.Y. Imanishi, R.D. Goldman, and J.E. Eriksson. 2014. Interphase phosphorylation of lamin A. *J. Cell Sci.* 127:2683–2696. http://dx.doi.org/10.1242/jcs.141820

Lane, S.I., H.-Y. Chang, P.C. Jennings, and K.T. Jones. 2010. The Aurora kinase inhibitor ZM447439 accelerates first meiosis in mouse oocytes by overriding the spindle assembly checkpoint. *Reproduction*. 140:521–530. http://dx.doi.org/10.1530/REP-10-0223

Leach, N.R., and R.J. Roller. 2010. Significance of host cell kinases in herpes simplex virus type 1 egress and lamin-associated protein disassembly from the nuclear lamina. *Virology*. 406:127–137. http://dx.doi.org/10.1016/j.virol.2010.07.002

Lemaitre, J.M., G. Géraud, and M. Méchali. 1998. Dynamics of the genome during early *Xenopus laevis* development: karyomeres as independent units of replication. *J. Cell Biol.* 142:1159–1166. http://dx.doi.org/10.1083/jcb.142.5.1159

Levy, D.L., and R. Heald. 2010. Nuclear size is regulated by importin α and Ntf2 in *Xenopus*. *Cell*. 143:288–298. http://dx.doi.org/10.1016/j.cell.2010.09.012

Levy, D.L., and R. Heald. 2012. Mechanisms of intracellular scaling. *Annu. Rev. Cell Dev. Biol.* 28:113–135. http://dx.doi.org/10.1146/annurev-cellbio-092910-154158

Mall, M., T. Walter, M. Gorjánácz, I.F. Davidson, T.B. Nga Ly-Hartig, J. Ellenberg, and I.W. Mattaj. 2012. Mitotic lamin disassembly is triggered by lipid-mediated signaling. *J. Cell Biol.* 198:981–990. http://dx.doi.org/10.1083/jcb.201205103

Maresca, T.J., and R. Heald. 2006. Methods for studying spindle assembly and chromosome condensation in *Xenopus* egg extracts. *Methods Mol. Biol.* 322:459–474. http://dx.doi.org/10.1007/978-1-59745-000-3_33

Marshall, W. 2002. Size control in dynamic organelles. *Trends Cell Biol.* 12:414–419. http://dx.doi.org/10.1016/S0962-8924(02)02341-3

Meshorer, E., and T. Misteli. 2006. Chromatin in pluripotent embryonic stem cells and differentiation. *Nat. Rev. Mol. Cell Biol.* 7:540–546. http://dx.doi.org/10.1038/nrm1938

Milbradt, J., R. Webel, S. Auerochs, H. Sticht, and M. Marschall. 2010. Novel mode of phosphorylation-triggered reorganization of the nuclear lamina during nuclear egress of human cytomegalovirus. *J. Biol. Chem.* 285:13979–13989. http://dx.doi.org/10.1074/jbc.M109.063628

Mochly-Rosen, D., K. Das, and K.V. Grimes. 2012. Protein kinase C, an elusive therapeutic target? *Nat. Rev. Drug Discov.* 11:937–957. http://dx.doi.org/10.1038/nrd3871

Muranyi, W., J. Haas, M. Wagner, G. Krohne, and U.H. Koszinowski. 2002. Cytomegalovirus recruitment of cellular kinases to dissolve the nuclear lamina. *Science*. 297:854–857. http://dx.doi.org/10.1126/science.1071506

Murray, A.W. 1991. Cell cycle extracts. *Methods Cell Biol.* 36:581–605. http://dx.doi.org/10.1016/S0091-679X(08)60298-8

Newport, J., and M. Kirschner. 1982a. A major developmental transition in early *Xenopus* embryos: I. characterization and timing of cellular changes at the midblastula stage. *Cell*. 30:675–686. http://dx.doi.org/10.1016/0092-8674(82)90272-0

Newport, J., and M. Kirschner. 1982b. A major developmental transition in early *Xenopus* embryos: II. Control of the onset of transcription. *Cell*. 30:687–696. http://dx.doi.org/10.1016/0092-8674(82)90273-2

Newton, A.C. 2003. Regulation of the ABC kinases by phosphorylation: protein kinase C as a paradigm. *Biochem. J.* 370:361–371. http://dx.doi.org/10.1042/BJ20021626

Nieuwkoop, P.D., and J. Faber. 1956. Normal table of *Xenopus laevis* (Daudin). A systematical and chronological survey of the development from the fertilized egg till the end of metamorphosis. North-Holland Publishing Co., Amsterdam. 243 pp.

Park, R., and J.D. Baines. 2006. Herpes simplex virus type 1 infection induces activation and recruitment of protein kinase C to the nuclear membrane and increased phosphorylation of lamin B. *J. Virol.* 80:494–504. http://dx.doi.org/10.1128/JVI.80.1.494-504.2006

Peter, M., J. Nakagawa, M. Dorée, J.C. Labbé, and E.A. Nigg. 1990. In vitro disassembly of the nuclear lamina and M phase-specific phosphorylation of lamins by cdc2 kinase. *Cell.* 61:591–602. http://dx.doi.org/10.1016/0092-8674(90)90471-P

Porwal, M., S. Cohen, K. Snoussi, R. Popa-Wagner, F. Anderson, N. Dugot-Senant, H. Wodrich, C. Dinsart, J.A. Kleinschmidt, N. Panté, and M. Kann. 2013. Parvoviruses cause nuclear envelope breakdown by activating key enzymes of mitosis. *PLoS Pathog.* 9:e1003671. http://dx.doi.org/10.1371/journal.ppat.1003671

Ron, D., and M.G. Kazanietz. 1999. New insights into the regulation of protein kinase C and novel phorbol ester receptors. *FASEB J.* 13:1658–1676.

Simon, D.N., and K.L. Wilson. 2013. Partners and post-translational modifications of nuclear lamins. *Chromosoma.* 122:13–31. http://dx.doi.org/10.1007/s00412-013-0399-8

Sims, J.R., S. Karp, and D.E. Ingber. 1992. Altering the cellular mechanical force balance results in integrated changes in cell, cytoskeletal and nuclear shape. *J. Cell Sci.* 103:1215–1222.

Sive, H.L., R.M. Grainger, and R.M. Harland. 2000. Early development of *Xenopus laevis*: a laboratory manual. Cold Spring Harbor Laboratory Press, Cold Spring Harbor, NY. 338 pp.

Soh, J.W., and I.B. Weinstein. 2003. Roles of specific isoforms of protein kinase C in the transcriptional control of cyclin D1 and related genes. *J. Biol. Chem.* 278:34709–34716. http://dx.doi.org/10.1074/jbc.M302016200

Speese, S.D., J. Ashley, V. Jokhi, J. Nunnari, R. Barria, Y. Li, B. Ataman, A. Koon, Y.T. Chang, Q. Li, et al. 2012. Nuclear envelope budding enables large ribonucleoprotein particle export during synaptic Wnt signaling. *Cell.* 149:832–846. http://dx.doi.org/10.1016/j.cell.2012.03.032

Sullivan, T., D. Escalante-Alcalde, H. Bhatt, M. Anver, N. Bhat, K. Nagashima, C.L. Stewart, and B. Burke. 1999. Loss of A-type lamin expression compromises nuclear envelope integrity leading to muscular dystrophy. *J. Cell Biol.* 147:913–920. http://dx.doi.org/10.1083/jcb.147.5.913

Toker, A. 1998. Signaling through protein kinase C. *Front. Biosci.* 3:D1134–D1147.

Webster, M., K.L. Witkin, and O. Cohen-Fix. 2009. Sizing up the nucleus: nuclear shape, size and nuclear-envelope assembly. *J. Cell Sci.* 122:1477–1486. http://dx.doi.org/10.1242/jcs.037333

Yanai, I., L. Peshkin, P. Jorgensen, and M.W. Kirschner. 2011. Mapping gene expression in two *Xenopus* species: evolutionary constraints and developmental flexibility. *Dev. Cell.* 20:483–496. http://dx.doi.org/10.1016/j.devcel.2011.03.015

Zink, D., A.H. Fischer, and J.A. Nickerson. 2004. Nuclear structure in cancer cells. *Nat. Rev. Cancer.* 4:677–687. http://dx.doi.org/10.1038/nrc1430